

# Growth of the Nanostructured Titanium Oxide by Anodization of Ti/Cu/Ti System

J.C. CHOJENKA\* AND A. ZARZYCKI

*Institute of Nuclear Physics, Polish Academy of Sciences, Radzikowskiego 152, 31-342, Krakow, Poland*

Doi: [10.12693/APhysPolA.145.147](https://doi.org/10.12693/APhysPolA.145.147)

\*e-mail: [juliusz.chojenka@ifj.edu.pl](mailto:juliusz.chojenka@ifj.edu.pl)

The study investigates the impact of the electrolyte composition and anodization conditions on titanium oxide microstructures, analyzing their influence on a trilayer titanium/copper/titanium system. The electrolytes used for anodization had different concentrations of ammonium fluoride and water. The quality and stability of the oxide growth were controlled by monitoring changes in the current density curves during anodization. In water-rich electrolytes, the titanium oxide layer exhibits improved structural quality but reduced layer conductivity, leading to electrical breakdown and destruction of the layer through rapid electrical discharge. Under equilibrium conditions between fluoride ions and water, scanning electron microscope images demonstrate nanoporous structures with inner pore diameters exhibiting a log-normal distribution, with median sizes ranging from 15 to 70 nm across voltage ranges. Linear correlations between the inner pore diameters and the applied voltage are observed, notably in certain electrolytes, indicating stable processes and high quality of the nanopatterned oxide.

topics: anodization, nanoporous titanium oxide, thin films, nanopatterning

## 1. Introduction

Nanostructured titanium oxide garners significant attention due to its potential applications in biomedical coatings [1], supercapacitors [2], solar cells [3], catalysis [4], templates for magnetic thin films [5], and spintronic devices [6,7]. This attention stems from the large surface-to-volume ratio in titanium oxide, its high surface activity accompanied by high sensitivity, and unique electronic structure.

Among the various methods for fabricating nanostructured metal oxides, one of the simplest and most effective is anodization — an electrochemical process enabling the creation of nanoporous or nanotubular oxides. Aluminum oxide stands as one of the extensively studied materials produced through this method. Anodized aluminum oxide (AAO) has been under study for several decades, leading to the optimization of obtaining highly ordered and tunable nanostructures in terms of diameter. This makes AAO a promising material as templates for the fabrication of functional materials with reduced dimensionality [8–12]. The successful development of an anodization-based process to generate nanotube arrays has extended from aluminum to other metallic or intermetallic materials, such as titanium oxide [13].

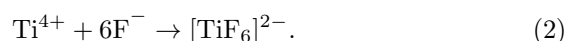
The anodization of the titanium may be described as a competition between the formation of oxide and the chemical dissolution of the oxide by fluoride ions [14]. For anodization to occur, the Ti film

should be submerged in the conductive electrolyte. In the absence of  $F^-$  ions in the media, a thin layer of titanium oxide, called barrier layer, is formed on the surface, according to the equation



The application of an electric field enhances this reaction by aiding the electrical transport of  $O^{2-}$  and  $Ti^{4+}$  ions through the growing oxide. However, the oxidation process is limited by the thickness of the oxide layer and slows down with its increase. As the oxide layer thickens, the ionic current decreases due to the formation of the  $Ti(OH)_xO_y$  hydroxide layer at the oxide/electrolyte interface. This layer is non-soluble and its surface is typically loose and porous, slowly inhibiting the diffusion of  $O^{2-}$  and  $Ti^{4+}$  ions.

The presence of fluoride ions in the electrolyte alters the oxidation process by complexing with the transported titanium cations at the oxide/electrolyte interface, preventing the precipitation of  $Ti(OH)_xO_y$ , i.e.,



Moreover, fluoride can react with titanium oxide and form water-soluble  $[TiF_6]^{2-}$  complexes, leading to the dissolution and breakdown of the barrier layer and an increase in electrical current in the initial stage of anodization. Under the electric field, the titanium oxide growth rate (1) and the dissolution rate (2) can achieve a balance, resulting in the steady growth of a porous or tubular titanium

TABLE I

Anodization parameters for different sample series.

Series	Concentration of $\text{NH}_4\text{F}$ [wt%]	Concentration of $\text{H}_2\text{O}$ [wt%]	Anodization voltage [V]
A	0.3	1.5	10,20,30,40,50
B	0.4	5	10,20,30,40,50
C	0.5	10	10,20,30,40,50

oxide layer. Eventually, the current can decrease due to various effects, such as reducing the diffusion of fluoride-containing species in and out of the pores/tubes [15].

Although the mechanism of titanium oxide growth during anodization is well-documented, the majority of research has been centered around work with titanium foil, which limits its application potential. The presence of a thick titanium foil underneath the oxide layer makes such a system unsuitable for use in microdevices. Additionally, the opacity of Ti metal diminishes its applicability for certain optical–electric devices, like dye-sensitized solar cells. Hence, there is a need for studies focusing on exploring methods to fabricate anodic  $\text{TiO}_2$  films on alternative functional substrates.

It is of significant importance to investigate the effect of the anodization conditions, because they play a crucial role in determining the microstructure of anodic films and will eventually determine their performances in the devices. In this paper, we will discuss the influence of the electrolyte composition on the microstructure of titanium oxide fabricated through the anodization of a trilayer system consisting of titanium/copper/titanium deposited on a silicon wafer. To the best of the authors’ knowledge, there are very few reports about comprehensive research on the influence of the anodization conditions on anodic  $\text{TiO}_2$  fabricated from multilayers.

## 2. Methods

The fabrication process of anodized titanium oxide (ATO) from thin films was divided into multiple stages. Firstly, we cut the silicon (100) wafer into 17 mm length squares, followed by sonication in acetone, isopropanol and distilled water. Then, a bilayer of Ti (50 nm)/Cu (100 nm) was deposited by e-beam evaporation in vacuum of  $10^{-5}$  mbar. Next, we placed a stencil mask at the center of the substrate to deposit 550 nm of Ti film in the shape of a 12 mm circle. This thick layer of titanium was used for the anodization process. The scheme depicting the sample fabrication process is shown in Fig. 1.

The anodization process was conducted in a homemade chamber with a platinum cathode and a titanium film as an anode. The distance between electrodes was set to 30 mm. Anodization was per-

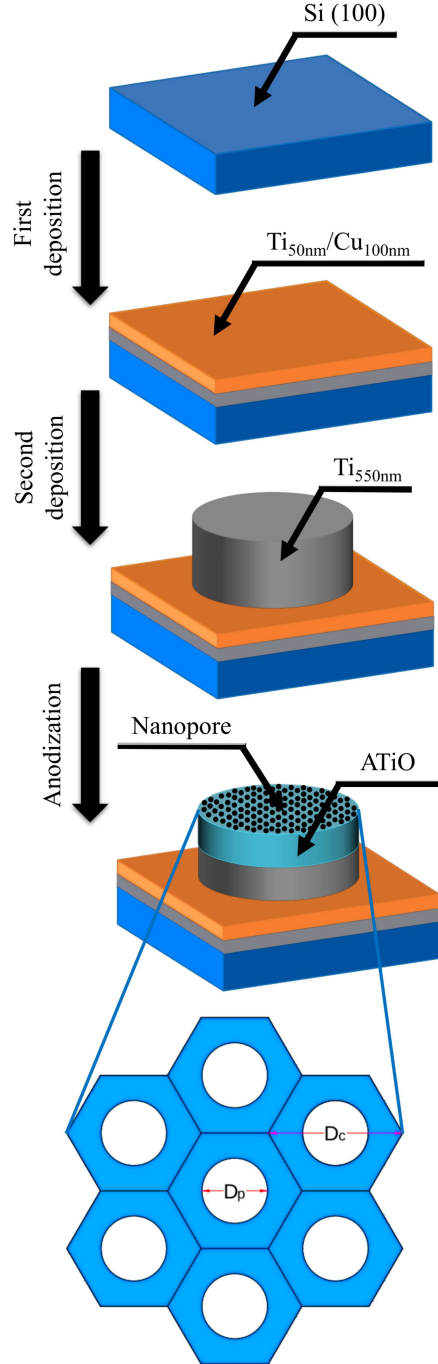


Fig. 1. The scheme of the sample fabrication process. The last picture shows schematic view of the anodized titanium oxide surface. Here,  $D_p$  is inner pore diameter and  $D_c$  is cell diameter.

formed in potentiostatic mode using a Delta Electronics SM 300-10D power supply, and the current was measured with an Agilent 34401A multimeter. The electrolytes for anodization consisted of ammonium fluoride, distilled water, and glycol ethylene. The chemical concentration of reagents and the anodization voltage used during the preparation process are listed in Table I. For clarity, we used code names for the samples, distinguishing them by

series denotation and anodization voltage, for example, A10, A20, etc. Anodization time ranged from 15 to 40 min. The surface morphology was studied by scanning electron microscope (SEM) imaging (Vega Tescan 3), and the chemical composition of the samples was determined through energy-dispersive X-ray spectroscopy (EDS) measurements (Bruker EDS detector).

### 3. Results

To understand the factors influencing the oxide growth process, we can employ the empirical kinetics equation for the anodization growth rate ( $r_g$ ), proposed by Cortes et al. [16],

$$r_g \propto AtF^2W^{-1} \exp(\alpha P) P + C(1 - \exp(\beta t))PW^{-1}, \quad (3)$$

where  $F$ ,  $W$ ,  $P$ , and  $t$  represent the fluoride concentration, water concentration, applied electrical potential, and time, respectively, and  $A$ ,  $C$ ,  $\alpha$ , and  $\beta$  are numerical constants. The growth rate of nanostructured titanium oxide is directly proportional to the square of the fluoride concentration, which results in increased dissolution of the oxide [17], and accounts for the increase in electrolyte conductivity [18]. The presence of water has an inverse effect compared to fluoride, decreasing the growth rate of titanium oxide. This reduction occurs due to the decrease in conductivity caused by a lower density of defects in the synthesized oxide [19].

Progress of anodization is typically monitored by changes in the current density  $j(t)$  curves. Figure 2 presents such  $j(t)$  dependences for anodized titanium films. Monitoring the change in electrical current density during the anodization process serves as a means of assessing the quality and stability of oxide layer growth. A typical  $j(t)$  curve for bulk titanium anodization consists of four parts: (i) barrier layer formation — characterized by a rapid decrease in current density, (ii) initiation of titanium oxide dissolution — marked by a minimum in current density, (iii) random etching of the titanium oxide surface to create nanopores — indicated by an increase in current density, and (iv) an equilibrium phase between the oxide growth and the dissolution, resulting in the stable formation of nanopores/nanotubes — evidenced by a constant current density or a linear decrease over extended anodization time.

During the initial few seconds of anodization, there is a rapid, exponential decrease in current density (Fig. 2), indicating stage (I) of the formation of an oxide barrier layer on the metallic surface of the anodized samples. Subsequently, the current densities for anodization of series A (Fig. 2a) and series B (Fig. 2b) exhibit primarily a linear dependence on the anodization time. This linear trend signifies a stable growth of the nanopatterned oxide layer, where the oxidation and dissolution processes reach equilibrium.

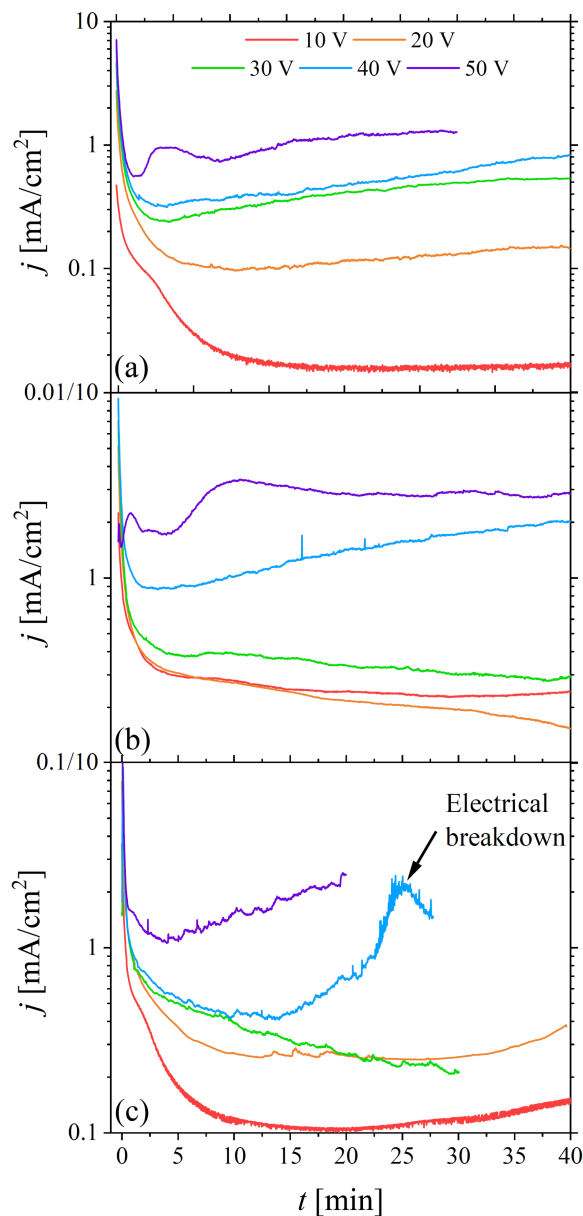


Fig. 2. Current density vs time during anodization process for different electrolytes compositions: (a) 0.3%  $\text{NH}_4\text{F}$ /1.5%  $\text{H}_2\text{O}$ /ethylene glycol, (b) 0.4%  $\text{NH}_4\text{F}$ /5%  $\text{H}_2\text{O}$ /ethylene glycol, (c) 0.5%  $\text{NH}_4\text{F}$ /10%  $\text{H}_2\text{O}$ /ethylene glycol and voltages 10–50 V. The current density is shown in the logarithmic scale.

A different scenario emerges for titanium films anodized in 0.5%  $\text{NH}_4\text{F}$ /10%  $\text{H}_2\text{O}$ /ethylene glycol of series C (Fig. 2c), where only small anodization voltages of 10 V and 20 V result in stable growth of titanium oxide. Higher anodization voltages exhibit irregularities in the current-density curves, indicating an uneven oxidation/dissolution process. This discrepancy becomes particularly evident at an anodization voltage of 40 V, where the rapid increase in current density suggests electrical breakdown throughout the titanium oxide layer.

TABLE II

Concentration of the elements from EDS.

Spot	C [%]	O [%]	F [%]	Si [%]	Ti [%]	Cu [%]
Green square	10.6	29.8	19.9	10.5	28.2	0.9
Red circle	15.0	3.0	0.6	80.4	1.0	0.0
Blue triangle	14.5	40.0	7.5	36.0	1.5	0.4

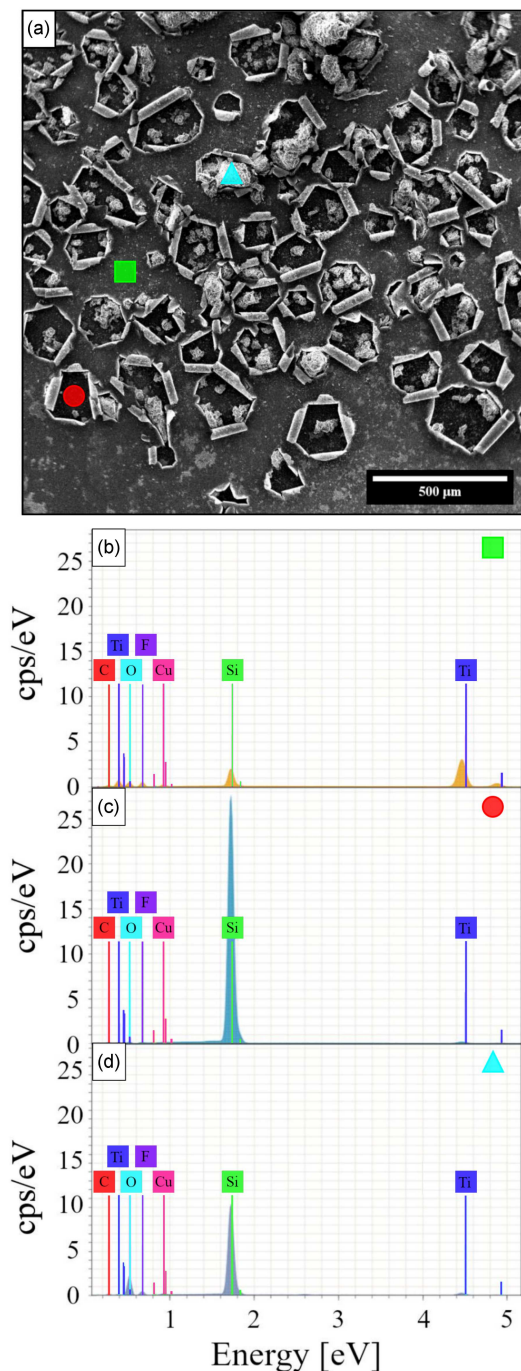


Fig. 3. SEM image of the electrical breakdown (a) for sample C40 and the EDS spectra for the different area on the sample: (b) green square, (c) red circle, (d) cyan triangle.

Electrical breakdown can cause partial exfoliation of the layer, resulting in the crater-like formation due to the electrical discharge from the layer to the substrate. Figure 3a displays the surface of an anodized titanium film (sample C40) after an electrical breakdown. The image reveals three discernible regions: a continuous layer (marked with a green square), a discharge crater (red circle), and irregular granules (cyan triangle).

To assess the elemental composition of these tree regions, we present EDS analysis in Fig. 3b–d. The spectrum corresponding to the continuous layer marked by a green square exhibits the expected elemental composition of anodized titanium oxide, primarily composed of titanium, oxygen, and fluoride (Fig. 3b). The small silicon peak in this spectrum is attributed to the substrate. Conversely, the spectrum of the adjacent red circle region displays a strong silicon peak and a lack of signal from other elements, indicating complete exfoliation of the layer due to electrical breakdown and discharge (Fig. 3c). In the EDS analysis of the last region, marked by a cyan triangle (Fig. 3d), the combination of silicon and oxygen peaks with minor traces of fluoride suggests the formation of  $\text{SiO}_2$  and/or  $\text{SiOF}$ . The quantitative EDS results are compiled in Table II.

Electrical breakdowns occur in samples from the C series, where anodization is conducted using a water-rich electrolyte. This process results in the growth of titanium oxide with a limited number of oxygen vacancies, thereby improving the structural quality of the layer. However, it also reduces the conductivity of the layer, where the titanium oxide layer behaves as a capacitor with opposite electrical charges at the top and bottom parts. An electrical current above a certain threshold potential will rapidly flow through the oxide layer, causing an electrical discharge and ultimately destroying the multilayer film. The exposed silicon substrate is susceptible to oxidation, enabling the formation of  $\text{SiO}_2$  or  $\text{SiOF}$  granules.

The surface images of samples anodized using different electrolytes at an anodization voltage of 30 V, in equilibrium between the oxidation and dissolution processes, are depicted in Fig. 4a–c, along with histograms of the inner pore diameters shown in Fig. 4d–f, respectively. Anodization of our trilayer system in 0.3%  $\text{NH}_4\text{F}$ /1.5%  $\text{H}_2\text{O}$ /ethylene glycol (Fig. 4a) and 0.4%  $\text{NH}_4\text{F}$ /5%  $\text{H}_2\text{O}$ /ethylene glycol (Fig. 4b) results in the formation of a nanoporous structure with the same pores diameter. However, in the case of the sample anodized in 0.5%  $\text{NH}_4\text{F}$ /10%  $\text{H}_2\text{O}$ /ethylene glycol (Fig. 4c), alongside nanopores of a slightly bigger diameter, large granules are also visible, and they are most likely  $\text{Ti}(\text{OH})_x\text{O}_y$ . The formation of hydroxyl granules on the titanium oxide surface is facilitated by the high water concentration in the electrolyte, while fluoride ions are insufficient to dissolve them efficiently.

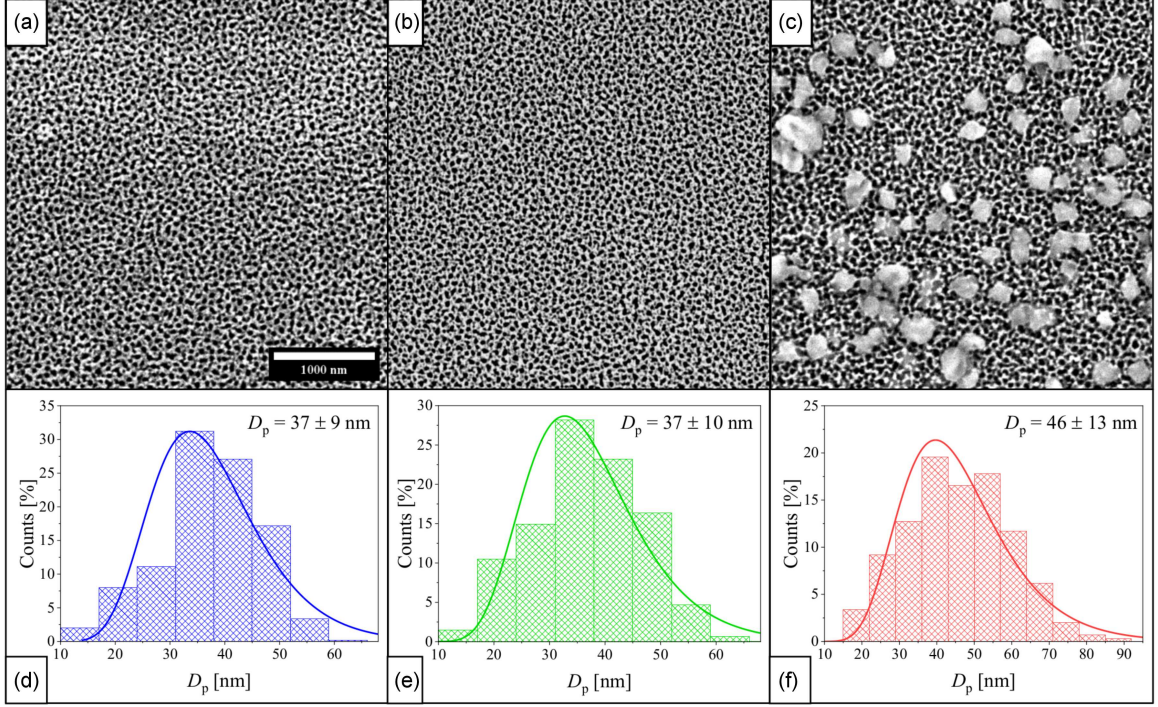


Fig. 4. SEM images for samples A30, B30, and C30 (a–c), together with histograms fitted with log-normal distributions of the inner pore diameter (d–f), respectively.

SEM analysis shows that the nanopores cover the surface homogeneously, but do not display short- or long-range spatial ordering. The arrangement of these nanopores is influenced for thin films by two key factors, i.e., the size of the titanium grains and the anodization time. An increase in anodization time contributes to a better spatial arrangement of nanopores. However, for thin layers, the anodization time must be reduced compared to bulk samples to prevent complete layer exfoliation after full oxidation. Furthermore, the average titanium grain size is smaller in thin film layers compared to bulk samples, which further limits the spatial order. Considering these two factors, the random distribution of nanopores across the titanium oxide is expected.

The histograms representing the inner pore diameters in Fig. 4d–e exhibit a log-normal distribution due to the nature of the measured values, which exclusively fall within positive real values. From our analysis of the inner pore diameters distribution, we determined the median pore diameter to be 37 nm for samples A30 and B30. The median is 46 nm in the case of the sample C30. However, considering the standard deviation, we can conclude that the pores diameter ( $D_p$ ) remains independent of the electrolyte composition.

The intricate interplay between ion concentration and titanium at the metal/electrolyte interface significantly influences the growth mechanism of titanium oxide, particularly in terms of nanotube length and structural quality. The applied potential

TABLE III

Fit parameters for the inner pore diameter as a function of anodization voltage.

Series	$y = ax + b$			
	$a$	$\Delta a$	$b$	$\Delta b$
A	0.48	0.29	18.35	10.79
B	1.14	0.14	5.30	3.95
C	0.53	0.21	23.71	6.90

stands as the primary factor influencing the inner pore diameters [20]. Figure 5 presents the influence of anodization voltage on these inner pore diameters for the trilayer Ti/Cu/Ti system anodized in various electrolytes.

We observed a linear increase in the inner pore diameters with increasing anodization voltage, where the nanopores are consistently present across the entire voltage range from 10 to 50 V. However, in series A (Fig. 5a) and C (Fig. 5c), the lowest voltage does not support the formation of nanopores in titanium oxide due to the imbalance between strong oxidation and insufficient dissolution of the formed oxide. Consequently, this imbalance results in nanopores with diameters of 0 nm being excluded from the fitting. The parameters obtained from the fittings are detailed in Table III.

The parameter ' $a$ ' stands for a factor describing the ratio of the increase in nanopore diameter to the voltage escalation. The parameter ' $b$ ' estimates the

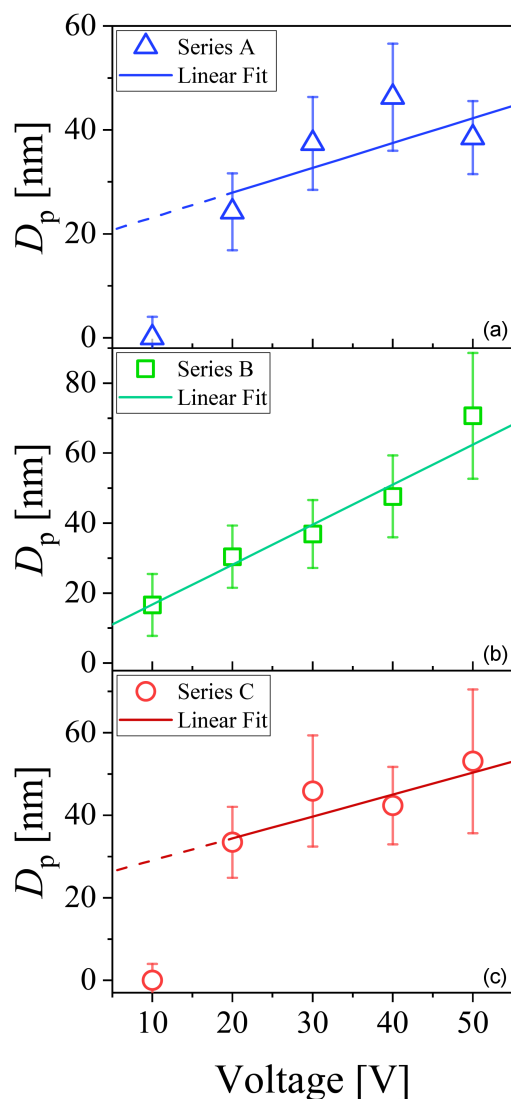


Fig. 5. The inner pore diameters vs anodization voltage for different electrolytes compositions (a) 0.3%  $\text{NH}_4\text{F}$ /1.5%  $\text{H}_2\text{O}$ /ethylene glycol, (b) 0.4%  $\text{NH}_4\text{F}$ /5%  $\text{H}_2\text{O}$ /ethylene glycol, (c) 0.5%  $\text{NH}_4\text{F}$ /10%  $\text{H}_2\text{O}$ /ethylene glycol.

interpolated nanopores size at zero voltage. However, nanopores start forming above a certain voltage threshold. For series A and C, this threshold exceeds 10 V, whereas for series B, it falls below 10 V.

In Table III we see that the nanopores size increase at a rate of approximately 0.5–1.0 nm per volt. The linear increase in the nanopore diameters may be an indicator of a stable process, and deviations from it suggest an imbalance between oxidation and dissolution parts of the anodization process. This divergence is notably evident in the series C (Fig. 5c), where the nanopores diameters appear relatively constant in relation to voltage. Non-linear characteristics indicate a process that may be challenging to control, resulting in difficulties achieving high-quality samples with the desired nanopattern.

The most consistent linear fit across the entire range from 10 to 50 V is observed in series B (Fig. 5b), suggesting that anodization of the trilayer Ti/Cu/Ti performed in 0.4%  $\text{NH}_4\text{F}$ /5%  $\text{H}_2\text{O}$ /ethylene glycol yields the most predictable results with the highest oxide quality.

#### 4. Conclusions

We examined the influence of the electrolyte composition and the applied voltage on the anodization process of the Ti/Cu/Ti trilayer. Our studies confirm the feasibility of fabricating nanopatterned titanium oxides with adjustable pore sizes from thin film anodization. The porous titanium oxide growth is significantly influenced by the ion concentration, especially from the abundance of water carrying the risk of electrical breakdown. Analysis of SEM images revealed that such breakdown events result in defoliation of the metallic trilayer in certain parts of the sample in the form of craters and the formation of granules of oxidized silicon species through the afterward anodization.

In electrolytes with moderate water ion concentrations, the anodization process yields porous titanium oxide with pore sizes linearly correlated to the applied voltage. The inner pore diameters follow a log-normal distribution, with median values ranging from 15 to 70 nm across voltages ranging from 10 to 50 V, respectively.

#### Acknowledgments

The support from the NCN grant 2015/19/D/ST3/01843 is gratefully acknowledged.

#### References

- [1] A. Bartkowiak, A. Zarzycki, S. Kac, M. Perzanowski, M. Marszałek, *Materials* **13**, 5290 (2020).
- [2] K. Siuzdak, R. Bogdanowicz, M. Sawczak, M. Sobaszek, *Nanoscale* **7**, 551 (2015).
- [3] L. Wang, Y. Wang, Y. Yang, X. Wen, H. Xiang, Y. Lia, *RSC Adv.* **5**, 41120 (2015).
- [4] J.E. Yoo, M. Altomare, M. Mokhtar, A. Alshehri, S.A. Al-Thabaiti, A. Mazare, P. Schmuki, *Phys. Status Solidi (a)* **213**, 2733 (2016).
- [5] J. Chojenka, A. Zarzycki, M. Perzanowski, M. Krupiński, T. Fodor, K. Vad, M. Marszałek, *Materials* **16**, 289 (2023).
- [6] A. Zarzycki, J. Chojenka, M. Perzanowski, M. Marszałek, *Materials* **14**, 2390 (2021).

- [7] J. Chojenka, A. Zarzycki, M. Perzanowski, T. Fodor, K. Mróz, V. Takáts, K. Vad, M. Krupinski, M. Marszałek, *J. Phys. Chem. C*, **128**, 375 (2024).
- [8] A. Maximenko, M. Marszałek, J. Chojenka, J. Fedotova, B.R. Jany, F. Krok, J. Morgiel, A. Zarzycki, Y. Zabala, *J. Magn. Magn. Mater.* **477**, 182 (2019).
- [9] T.N. Anh Nguyen, J. Fedotova, J. Kasiuk, V. Bayev, O. Kupreeva, S. Lazarouk, D.H. Manh, D.L. Vu, S. Chung, J. Åkerman, V. Altynov, A. Maximenko, *Appl. Surf. Sci.* **427B**, 649 (2018).
- [10] S. Xu, Y. Lei, *ChemPlusChem* **83**, 741 (2018).
- [11] Q. Xu, G. Meng, F. Han, *Prog. Mater. Sci.* **95**, 243 (2018).
- [12] M. Krupinski, M. Perzanowski, A. Maximenko, Y. Zabala, M. Marszałek, *Nanotechnology* **28**, 194003 (2017).
- [13] K. Lee, A. Mazare, P. Schmuki, *Chem. Rev.* **114**, 9385 (2014).
- [14] G.K. Mor, O.K. Varghese, M. Paulose, N. Mukherjee, C.A.J. Grimes, *Mater. Res.* **18**, 2588 (2003).
- [15] G.K. Mor, O.K. Varghese, M. Paulose, K. Shankar, C.A. Grimes, *Sol. Energy Mater. Sol. Cells* **90**, 2011 (2006).
- [16] F.J.Q. Cortes, P.J. Arias-Monje, J. Phillips, H. Zea, *Mater. Design* **96**, 80 (2016).
- [17] Z.B. Xie, D.J. Blackwood, *Electrochim. Acta* **56**, 905 (2010).
- [18] K. Lee, J. Kim, H. Kim, Y. Lee, Y. Tak, *J. Korean Phys. Soc.* **54**, 1027 (2009).
- [19] K.S. Raja, T. Gandhi, M. Misra, *Electrochem. Commun.* **9**, 1069 (2007).
- [20] H. Sopha, L. Hromadko, K. Nechvilova, J.M. Macak, *J. Electroanal. Chem.* **759**, 122 (2015).